Structures and Transport Properties of Hydrated Water-Soluble Dendrimer-Grafted Polymer Membranes for Application to Polymer Electrolyte Membrane Fuel Cells: Classical Molecular Dynamics Approach

Seung Soon Jang and William A. Goddard III*

Materials and Process Simulation Center (MC 139-74), California Institute of Technology, Pasadena, California 91125

Received: September 14, 2006; In Final Form: November 1, 2006

We investigate a new molecular architecture in which water-soluble dendrimers are grafted onto a linear polymer for application to polymer electrolyte membrane fuel cells (PEMFC). Using full-atomistic molecular dynamics simulations, we examined the nanophase segregation and transport properties in hydrated membranes with this new architecture. In order to determine how the nature of the linear polymer backbone might affect membrane properties, we considered three different types of linear polymers, poly(epichlorohydrin) (PECH), polystyrene (PS), and poly(tetrafluoroethylene) (PTFE), each in combination with the second-generation sulfonic polyaryl ether dendrimer to form PECH-D2, PS-D2, and PTFE-D2. Our simulations show that the extent of nanophase segregation in the membrane increases in the order of PECH-D2 (∼20 Å) < PS-D2 (∼35 Å) < PTFE-D2 (∼40 Å) at the same water content, which can be compared to ∼30−50 Å for Nafion and ∼30 Å for Dendrion at the same water content. We find that the structure and dynamics of the water molecules and transport of protons are strongly affected by the extent of nanophase segregation and water content of the membrane. As the nanophase-segregation scale increases, the structure in water phase, the water dynamics, and the proton transport approach those in bulk water. On the basis of the predicted proton and water transport rates, we expect that the PTFE-D2 may have a performance comparable with Nafion and Dendrion.

1. Introduction

Enormous efforts have been and continue to be expended toward developing improved polymer electrolyte materials for polymer electrolyte membrane fuel cells (PEMFC).[1−6] This has led to a number of new materials, but Nafion continues to be considered the material of choice because of its high proton conductivity (0.1 S/cm at 80 °C and 100% relative humidity) and its excellent chemical and thermal stability.[7−10] Even so, there continues to be a need to find alternative materials that can perform well at higher temperatures (120 °C or above).

Recently, we proposed a strategy for improving the performance of PEMFC by utilizing a dendritic molecular architecture having the following favorable features:[11] (i) a well controlled nanoscale segregation of the hydrophilic acid containing regions arising from the monodisperse molecular weight distribution achievable by the stepwise iterative synthetic route used for dendrimers and (ii) the controllability of the distribution of the terminal acid groups at the periphery (or surface) of the dendrimer by the specific choices in the monomers from which the dendrimer is constructed.

We considered that this direct control over the spacing in the hydrophilic regions could allow designs in which the water solvent could be retained in the membrane at temperatures above 100 °C.

Our previous studies on Dendrion allowed us to make a very simple choice for the hydrophobic polymer backbone to which the dendrimer is attached. Now, we want to consider the issue of the optimum choice of the polymer backbone. An advantage of the Dendrion concept is that the dendrimer controls the sizes of the hydrophilic domains independently of the nature of the polymer backbone, which determines the spatial distribution of these hydrophilic domains and the nature of the hydrophobic domains. In contrast, for Nafion, the nanophase distribution of hydrophilic and hydrophobic domains and the positioning of the acid groups within these domains are complex functions of the branching and monomers of the polymer backbone.

Thus, we consider here three different types of linear backbone polymers, poly(epichlorohydrin) (PECH, Figure 1a), polystyrene (PS, Figure 1b), and poly(tetrafluoroethylene) (PTFE, Figure 1c), to each of which the same the water-soluble dendrimer is grafted, as shown in Figure 2.

In order to assess how the nanophase segregation and transport in the hydrated membrane depend on the type of backbone polymer, we predict the membrane structure consists of dendrimer-grafted polymers with 10 and 20 wt % of water content. The results for these dendrimer-grafted polymer systems are compared with the properties of a Nafion membrane and Dendrion membrane calculated using the same simulation techniques.[11,12]

2. Simulation Details

All simulations were carried out using a full-atomistic model of the second-generation polyaryl ether dendrimer-grafted copolymers as shown in Figure 2. The degree of polymerization of each backbone polymer was determined to have an equivalent weight of ∼650.

2.1. Force Field. We used the DREIDING force field (FF)[13] as previously used to study Nafion[12,14−17] and Dendrion[11] except that the fluorocarbon parts were described using recently optimized force field[18] parameters and the water was described using the F3C force field.[19] These force field parameters are described in the original papers[13,18,19] and in our previous study[12]

10.1021/jp066014u CCC: $37.00 © 2007 American Chemical Society
Published on Web 01/20/2007

on hydrated Nafion. Thus, the force field has the form

$$E_{\text{total}} = E_{\text{vdW}} + E_{\text{Q}} + E_{\text{bond}} + E_{\text{angle}} + E_{\text{torsion}} + E_{\text{inversion}} \quad (1)$$

where E_{total}, E_{vdW}, E_{Q}, E_{bond}, E_{angle}, E_{torsion}, and $E_{\text{inversion}}$ are the total energies and the van der Waals, electrostatic, bond stretching, angle bending, torsion, and inversion components, respectively.

The individual atomic charges of the copolymer were assigned using the charge equilibration (QEq) method[20] optimized to reproduce Mulliken charges of small molecules. The atomic charges of the water molecule were from the F3C water model.[19] The particle−particle particle−mesh (PPPM) method[21] was used to calculate the electrostatic interactions.

2.2. Molecular Dynamics. All of the annealing and molecular dynamics (MD) simulations were performed using the MD code LAMMPS (large-scale atomic/molecular massively parallel simulator) from Plimpton at Sandia[22,23] with modifications to handle our force fields.[11,12,24] The equations of motion were integrated using the velocity Verlet algorithm[25] with a time step of 1.0 fs. The Nose−Hoover temperature thermostat for the canonical ensemble (NVT) and isobaric−isothermal ensemble (NPT) MD simulations used the damping relaxation time of 0.1 ps and the dimensionless cell mass factor of 1.0.

2.3. Simulation Cells. We constructed hydrated membrane systems for each kind of backbone polymer using two water concentrations of 10 wt % and 20 wt % as summarized in Table 1. (i) The 20 wt % case contains three identical dendrimer-grafted copolymer chains and 480 water molecules (including 48 hydronium molecules), corresponding to an average of 10 water molecules per each acid group. (ii) The 10 wt % case contains the same amount of dendrimer-grafted copolymer chains and 240 water molecules (including 48 hydronium molecules), corresponding to 5 water molecules per acid group.

We expect all of the 48 sulfonic acid groups in the membrane to be ionized. Here, it should be stressed that the degree of hydration is critical in determining the extent of the ionization. In the case of the perfluorosulfonic acid (PFSA) such as Nafion, it has been observed via IR technique[26] that the PFSA is fully ionized at water contents of at least 2 H_2O/SO_3H. In our systems with *para*-toluene sulfonic acid in dendrimer, we had water contents of 5 and 10 H_2O/SO_3H. It is known that the experimental pK_a ranges from −3.0 to −2.6, and it should be noted that just one non-ionized sulfonic acid group would lead to p$K_a = \sim -1.8$ to −1.5 for this water-content condition. Thus, we believe that assuming full ionization of all sulfonic acid groups is reasonable for this system. To provide a measure of the statistical uncertainties, all data in this paper were obtained from two independent samples for each backbone polymer with 10 wt % and 20 wt % of water content using different initial configurations.

In addition to the simulations described above, we constructed eight-times-larger systems by making a $2 \times 2 \times 2$ superstructure of the smaller systems and implemented independent simulations to investigate the characteristic dimension of phase segregation and to analyze characteristic dimensions. These larger scale calculations used 24 dendrimer-grafted polymer chains and 3840 water molecules in the simulation cell for 20 wt % of water content. However, the dynamical properties (e.g., diffusion) reported here are based on the smaller system.

2.4. Construction and Equilibration of the Amorphous Membrane. The time scales for the relaxation of polymers are extremely slow, far too slow for standard equilibrium MD to evolve to the equilibrium structure. In order to obtain well-equilibrated structures for complex amorphous polymers with a minimum of effort, we have developed a general annealing procedure which accelerates the attainment of equilibrium by driving the system repeatedly through cycles of thermal annealing (between 300 and 600 K) and pressure annealing (between densities of 0.5 to densities of 1.1 times the expected density). This procedure aims to help the system to quickly escape from various local minimums to find the globally better structures, and for heterogeneous systems, it promotes the migration of species required for optimum phase segregation.

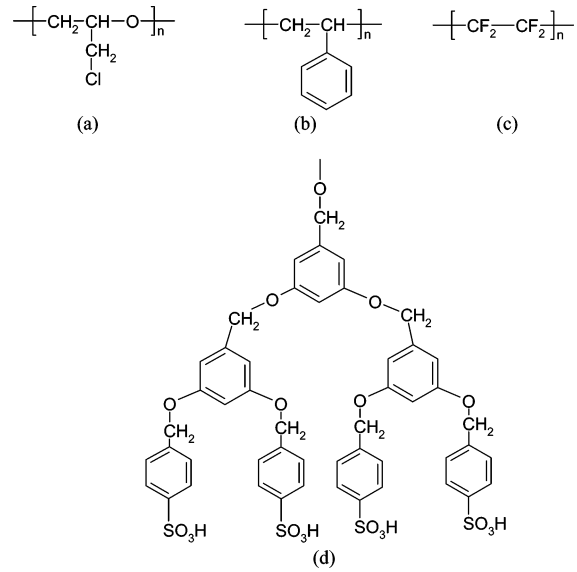

Figure 1. Chemical structures of backbone polymers and dendrimer: (a) poly(epichlorohydrin), PECH; (b) polystyrene, PS; (c) poly-(tetrafluoroethylene), PTFE; and (d) the second-generation polyaryl ether dendrimer with four sulfonic acid groups.

The steps in the annealing procedure are as follows: (a) Use Monte Carlo (MC) techniques to construct the initial three-dimensional amorphous structure of each dendrimer-grafted copolymer membrane using periodic boundary conditions (these studies used the Amorphous Builder of Cerius2, [27] but the results are not sensitive to the particular flavor of MC). In this step, the van der Waals radii were reduced by 70% to favor formation of extended polymer structures. (b) Gradually expand the initial cell by 50% over a period of 50 ps while the temperature is simultaneously increased from 300 to 600 K. (c) Equilibrate at 600 K for 50 ps using fixed density ($\rho = 0.5\rho_0$) NVT MD. (d) Gradually compress the system back to a density of $\rho = 1.1\rho_0$ over 50 ps while cooling the temperature down to the target temperature ($T = 300$ K). (e) Repeat steps b to d five times. (f) At the original target density ($\rho_0 = 1.5$ g/cm^3), equilibrate for 100 ps of NVT MD (fixed volume and Nose−Hoover thermostat[28] at 300 K). (g) Finally, allow the density to optimize with 5 ns NPT MD at 1 atm to fully equilibrate the density and structure at the target temperature (353.15 K).

This annealing equilibration procedure was used in exactly the same way in our previous studies of Nafion[12] and Dendrion.[39] This annealing procedure achieves a fully equilibrated system at the target temperature and pressure. We emphasize here that we do *not* bias the predicted structure by imposing any particular geometry (cylinders, spheres, lamellae) for the distribution of water in the system, nor do we impose any particular density or packing. Rather, the strategy of temperature and pressure MD annealing is designed to obtain an equilibrated distribution of water in an equilibrated polymer system at target conditions (in this case, 353.15 K and 1 atm).

This led to a final density of each dendrimer-grafted polymer as summarized in Table 1.

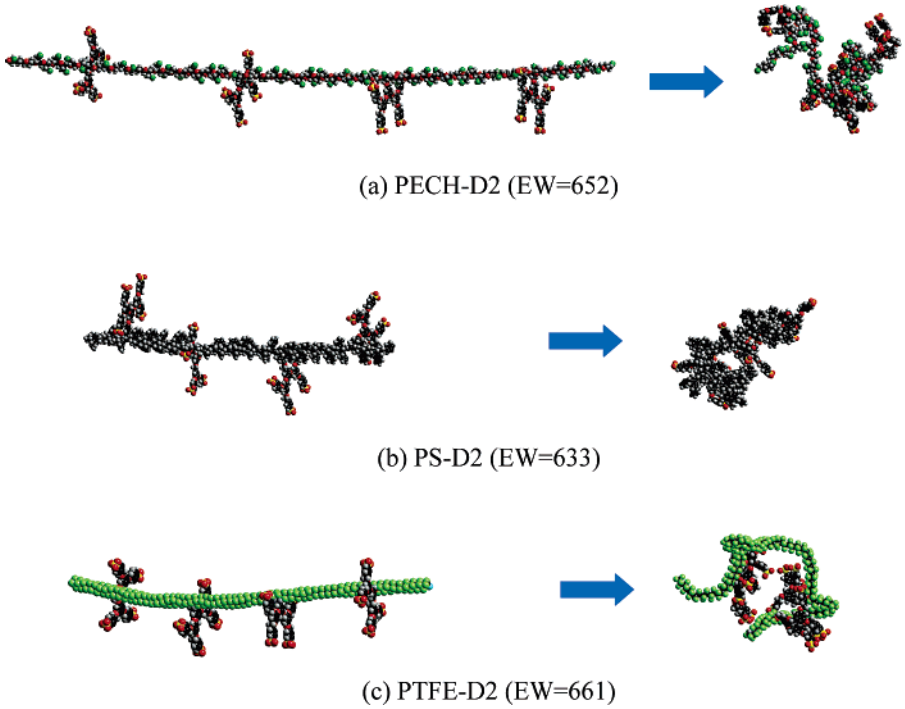

Figure 2. Full-atomistic models of the second-generation polyaryl ether dendrimer-grafted polymers. The number of dendrimers per chain is the same for all cases, and the values in the parentheses denote the equivalent weight for each polymer. The conformations in the right-hand side are equilibrated ones from their hydrated membranes.

TABLE 1: Composition and Densities of Simulated Hydrated Dendrimer-Grafted Copolymer

	PECH-D2		PS-D2		PTFE-D2	
molecular weight	10430		10130		10614	
equivalent weight	652		633		661	
no. of sulfonate groups			48			
no. of chains			3			
temperature (K)			353.15			
no. of water	240	480	240	480	240	480
(H_2O/SO_3H)	(5)	(10)	(5)	(10)	(5)	(10)
water content (wt %)	10	20	10	20	10	20
density (g/cm^3)	1.22 ± 0.01	1.22 ± 0.01	0.98 ± 0.01	1.06 ± 0.01	1.49 ± 0.01	1.42 ± 0.01
volume (Å^3)	49730 ± 360	55960 ± 280	61270 ± 440	63000 ± 380	38870 ± 280	45790 ± 340

2.5. Calculation of Properties. After completing step g of the annealing, we equilibrated the system using NPT MD simulations for another 5 ns at 353.15 K for use in calculating properties. This is the operating temperature of Nafion based PEMFC that was used in our previous simulations, allowing us to compare the properties of the dendrimer-grafted polymer directly with those of the Nafion and the Dendrion.

We used the trajectory file for this full 5 ns NPT calculation to calculate such properties as density and pair correlation functions.

In order to obtain the larger scale required to analyze the scattering factor, we extended the periodic cell by a factor of two in each direction applying periodic boundary conditions only for the extended cell. For these larger systems, we repeated steps b−f of the annealing procedure but performed step g only for 400 ps of the NPT MD simulation. During this temperature−pressure annealing procedure with five cycles, the nanophase-segregated morphology of each system does not undergo a significant change, indicating that each system reaches its stable morphology during the annealing procedure. In regard to the periodicity of morphology that is retained after the severe annealing procedure, we believe that this may be a characteristic of the nanophase segregation of graft copolymers.

3. Results and Discussion

Figure 3 presents snapshots of the final frame from the NPT MD simulations which show that water molecules are well-associated with the water-soluble dendrimer and form water phase. A noticeable difference is observed among PECH-D2, PS-D2, and PTFE-D2 with respect to the structure and dimension of the hydrated membrane. These differences seem to be strongly influenced by the type of backbone polymer even under the same conditions in terms of molecular weight, equivalent weight, and water content. This shows that the nature of the polymer backbone affects both the packing of the backbone and the spacing of the dendritic regions. This section analyzes the properties of the membrane and compares the affects of each type of backbone polymer.

3.1. Background on Nanophase Segregation. A general consensus from experiments[2,29−43] and simulations[14−16,44−51] is that an important factor in the favorable properties of Nafion based PEMFC is its nanophase-segregated structure, which consists of a percolating hydrophobic phase of perfluorinated polymer backbone interspersed with a percolating water phase associated with the sulfonic acid groups of the polymer.

In a previous study,[12] we showed that the characteristic dimensions of the nanophase-segregated structure in the Nafion

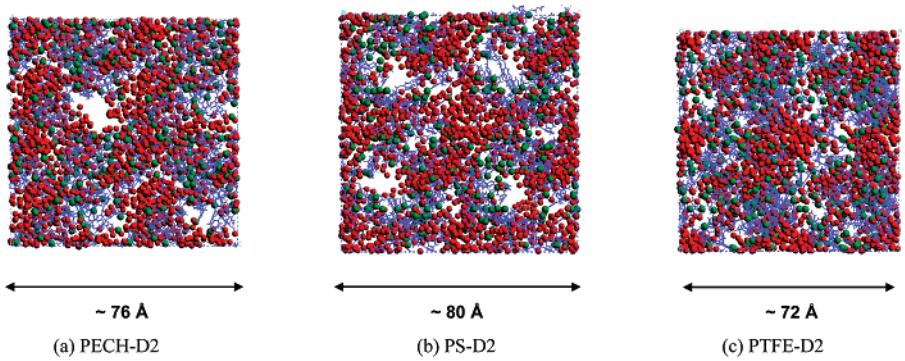

Figure 3. Nanophase-segregated structures of the hydrated dendrimer-grafted copolymer membrane with 20 wt % water content predicted from the simulations at 353.15 K. Blue components denote dendrimer, green balls denote the sulfur atoms, and red balls denote the oxygen atoms of water molecules. For clarity, the backbone polymer chains are not shown.

membrane can be controlled by the specific monomeric sequence of the Nafion polymer chain, which in turn affects the water/proton transport characteristics of PEMFC. Although the monomeric sequences of the Nafion chain in this previous study were quite simplified, this study focused on the molecular architecture as a variable affecting the final performance of PEMFC.

On the basis of these insights about the origins of the favorable properties of Nafion for PEMFC, we have suggested that it might be possible to improve the performance of PEMFC by utilizing a dendritic molecular architecture that has the favorable features mentioned above.[11] We find that the distances between acid groups are predictable and controllable because of their covalent connectivity to the dendrimer. Thus, it seems reasonable that we can systematically harness the nanophase segregation in a membrane by introducing this interesting architecture with an appropriate size. Indeed, in our previous study,[11] we presented the nanophase segregation and transport properties of Dendrion as a new class of copolymer consisting of the water-soluble polyaryl ether Fréchet dendrimer[52] and the linear PTFE.

This study expands this idea to enhance our capability to systematically harness the nanophase segregation in PEMFC. Thus, while using such an interesting dendritic molecular architecture as an essential component, we focus on the backbone polymer as another variable affecting membrane properties such as nanophase segregation and transport because of the variations in interaction between backbone polymer and water.

3.2. Correlations of Acid Group. Figure 4 shows the pair correlation functions for sulfur−sulfur pairs, $g_{S-S}(r)$. This pair correlation function, $g_{A-B}(r)$, indicates the probability density of finding A and B atoms at a distance r, averaged over the equilibrium trajectory as in eq 2

$$g_{A-B}(r) = \frac{\left(\dfrac{n_B}{4\pi r^2\,dr}\right)}{\left(\dfrac{N_B}{V}\right)} \tag{2}$$

where n_B is the number of B particles located at the distance r in a shell of thickness dr from particle A, N_B is the number of B particles in the system, and V is the total volume of the system.

This pair correlation analysis (Figure 4) shows maxima of g_{S-S} = 4.7 Å for 10 wt % H_2O and g_{S-S} = 4.9 Å for 20 wt % H_2O for PECH-D2 and g_{S-S} = 4.7 Å for 10 wt % H_2O and g_{S-S} = 4.9 Å for 20 wt % H_2O for PS-D2 with similar

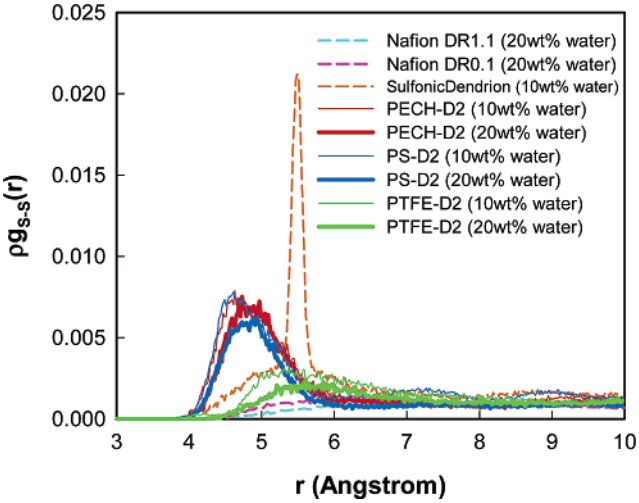

Figure 4. Pair correlation function of the sulfonic acid group in the hydrated membranes. The $g_{S-S}(r)$ for Nafion and Dendrion was reported previously.[11,12] ρ indicates the number density of sulfur.

distributions of sulfonic acid groups and almost the same peak position for both of water content.

This is a much closer S−S distance than that observed in our previous simulations: Nafion (∼6−7 Å) for 20 wt % H_2O[12] and Dendrion (5.5 Å) for 10 wt % H_2O.[11] In contrast, for PTFE-D2, we found g_{S-S} = 5.3 Å for 10 wt % H_2O and g_{S-S} = 5.6 Å for 20 wt % H_2O which is larger than those for PECH-D2 and PS-D2.

The overall distribution of S−S distances for PTFE-D2 is much broader than for PECH-D2 and PS-D2. To understand the origin of this difference, we decomposed the total $\rho g_{S-S}(r)$ into the contribution from acid pairs belonging to the same dendrimer (intra-dendrimer) and the contribution from acid pairs belonging to different dendrimers (inter-dendrimer) as shown in Figure 5. Here, we see that the PECH-D2 (Figure 5a) and the PS-D2 (Figure 5b) have more intra-dendrimer contributions for a S−S distance < 5 Å than PTFE-D2 (Figure 5c).

From this decomposition of $\rho g_{S-S}(r)$ in Figure 5, we found that the dominant correlation distance between sulfonate groups is nearly the same for both inter-dendrimer and intra-dendrimer, indicating that the dendrimers are in sufficiently close contact with each other and that the sulfonic acid distributions are uniform. We expect that this characteristic would help the membrane retain a continuous hydrophilic water phase in the nanophase-segregated morphology providing efficient proton-transfer rates. To clarify this point, Figure 6 shows connections between sulfur atoms of sulfonate groups within a 7 Å distance of each other. This shows a well-interconnected sulfur network

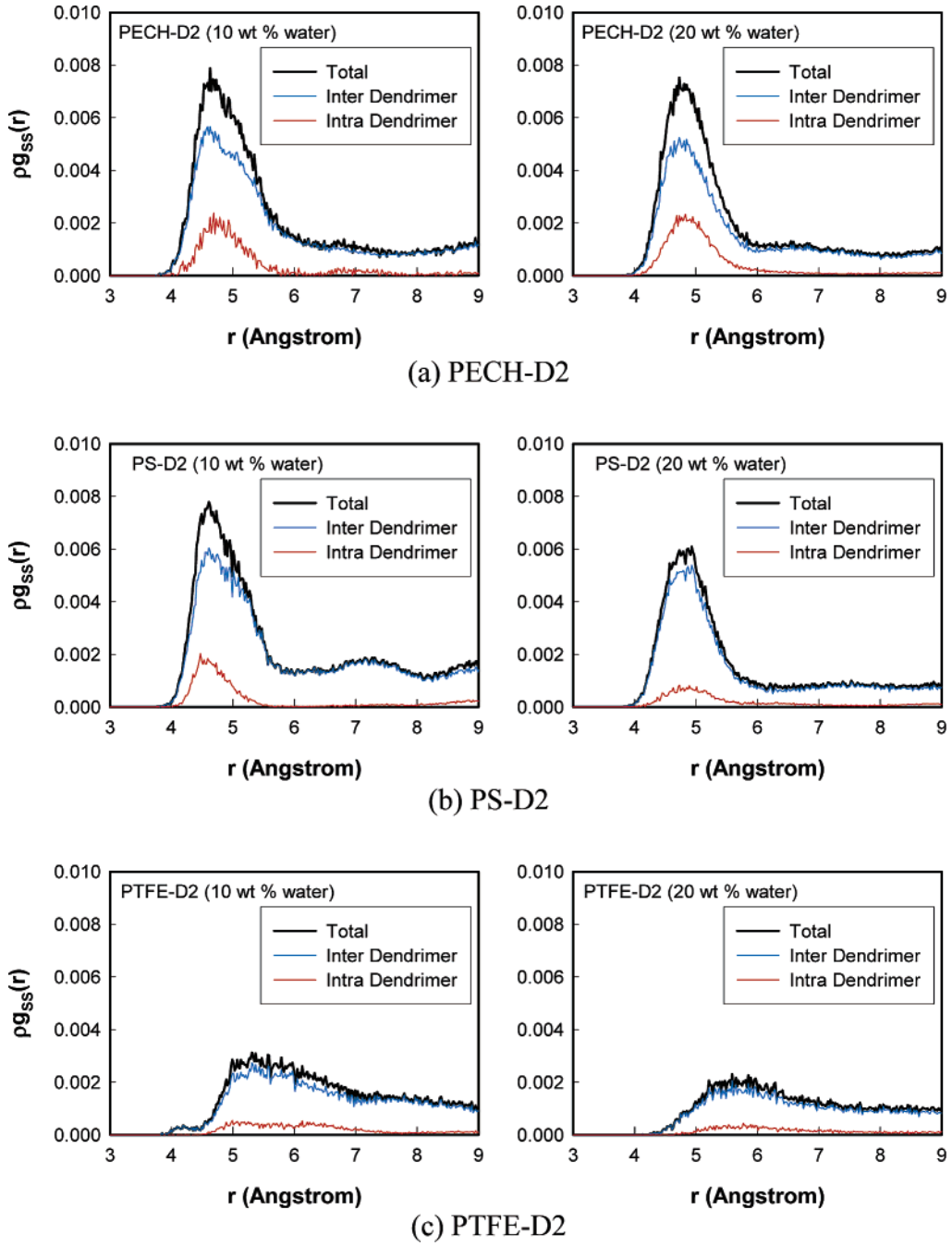

Figure 5. Decomposition of the pair correlation function of the acid group. "Inter Dendrimer" denotes the contribution from the pair of sulfonic acid groups belonging to different dendrimers whereas "Intra Dendrimer" denotes that from the pair of sulfonic acid groups belonging to the same dendrimer.

for all cases, indicating that dendrimers contact each other to form a percolated structure.

Figure 5 shows that $\rho g_{S-S}(r)$ is not significantly affected by the water content. Thus, increasing the water content by 100% increases the average S−S distance by 4% (∼0.2−0.3 Å). As discussed previously,[11] we believe that this insensitivity of $\rho g_{S-S}(r)$ to the water content results from the structural characteristics of the dendrimer in which the terminal sulfonate groups are locally concentrated through covalent connectivity in a well-defined structure. We consider this to be a positive aspect in retaining a constant structure during the fuel cell operation which may undergo a significant fluctuation in water content.

3.3. Structure of the Water in the Membrane. The characteristics of the water phase in the hydrated membrane are most important to the fuel cell performance since the proton transfer occurs through the water phase. Extensive studies on the proton transfer in water[53−62] and in polymer electrolyte membranes[3,55−57,63−65] have led to the general consensus that the proton diffusion rate in bulk water is approximately four to eight times larger than in the hydrated membrane. As summarized by Kreuer[55,57] and by Paddison,[3] this is attributed to the bulk water having a well-organized and compact hydrogen bonding network that aids efficient proton hopping. In contrast, the hydrated membranes have a reduced hydrogen bond connectivity. Specifically, Paul and Paddison described this aspect from the viewpoint of dielectric saturation of water by analyzing the restricted dynamics of water's dipole moment in the vicinity of anionic groups through their molecular statistical mechanical model.[66]

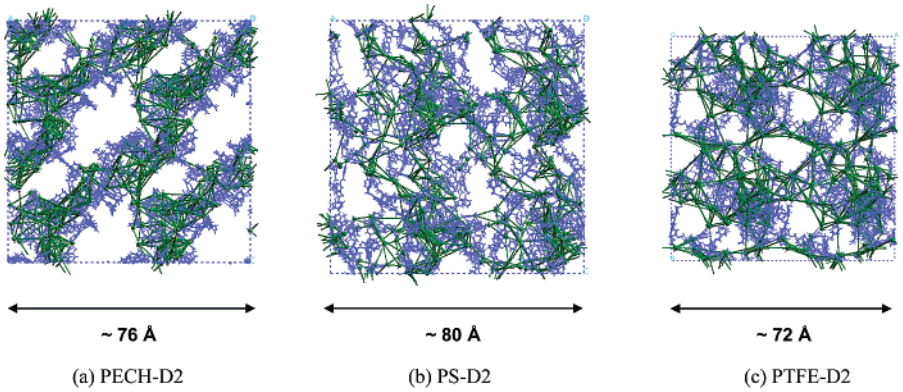

Figure 6. Distribution of sulfurs in sulfonic acids with 20 wt % of water content. The bonds are generated between sulfur atoms within 7 Å.

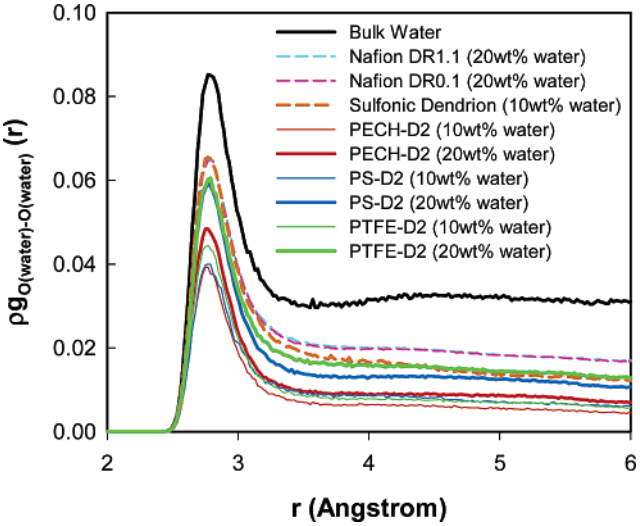

Figure 7. Product of pair correlation functions of water oxygens, $g_{O(water)-O(water)}(r)$ with water number density (ρ).

In order to characterize the structure in the water phase dispersed within a hydrated membrane, we calculated $\rho g_{O(water)-O(water)}(r)$ (see Figure 7). For comparison, the cases of bulk water and the results from our previous studies on the Nafion and the Dendrion are also included here. For the bulk water phase, we calculated a water coordination number of $CN_{H_2O} = 4.59$, in very good agreement with the value of $CN_{H_2O} = 4.5$ computed from neutron diffraction experiments.[67] We also calculated the average water coordination number for all cases simulated in this study as summarized in Table 2. For the dendrimer-grafted polymers PECH-D2, $CN_{H_2O} = 1.75$ for 10 wt % H_2O and $CN_{H_2O} = 2.37$ for 20 wt % H2O; PS-D2, $CN_{H_2O} = 1.92$ for 10 wt % H_2O and $CN_{H_2O} = 2.97$ for 20 wt % H2O; and PTFE-D2, $CN_{H_2O} = 2.01$ for 10 wt % H_2O and $CN_{H_2O} = 3.16$ for 20 wt % H_2O. Obviously, the structure of the water phase in the membranes approaches a bulk-water-like structure with increasing water content.

Of course the structure of the water phase is affected by the type of backbone polymer. Thus, the attractive interactions of water with a hydrophilic backbone polymer may perturb the structure in the water phase more than with a hydrophobic backbone (for a given water content) because water molecules can associate more strongly with hydrophilic backbone polymers in comparison with hydrophobic ones. Since the three types of dendrimer-grafted polymer membranes were simulated under the same conditions, including equivalent weight, dendrimer structure, water content, and temperature, we may infer that the structural difference in water phase observed in our simulations is attributed to the difference in the interaction between water and backbone polymer. Indeed, Figure 8 shows that the attractive interaction of backbone polymer with water molecules decreases in the order of PECH-D2 > PS-D2 > PTFE-D2 for both water contents. We attribute this relatively more attractive interaction of the PECH-D2 backbone with water to the hydrophilicity of epichlorohydrin (the monomeric unit of the PECH-D2 backbone). Thus, the hydrophilic PECH can absorb a certain amount of water even without a hydrophilic dendrimer as shown.[68]

However, the results in Table 2 raise the question as to why the coordination numbers of water in the dendrimer-grafted

TABLE 2: Water Coordination Number for Water in Membrane

system		water content (wt %)	water coordination number
bulk water			4.59 (exptl 4.5)
PECH-D2		10	1.75
		20	2.37
PS-D2		10	1.92
		20	2.97
PTFE-D2		10	2.01
		20	3.16
Nafion	dispersed DR = 1.1	20	3.85[a]
	blocky DR = 0.1	20	3.82[a]
sulfonic dendrion		10	3.40[a]

[a] References 11 and 12.

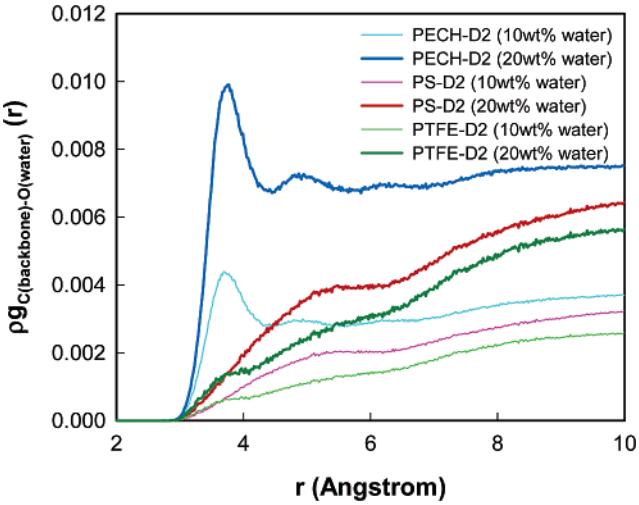

Figure 8. Product of pair correlation functions of carbon in the backbone polymer and water oxygen, $g_{C(backbone)-O(water)}(r)$ with water number density (ρ).

polymers are smaller than those in the Nafion (~3.82−3.85) and the sulfonic Dendrion (3.40). Thus, even though PTFE-D2 has exactly the same kind of backbone polymer (PTFE) used in the Nafion and the Dendrion, the water coordination number of water for the PTFE-D2 is smaller than that for the Nafion (3.16 for the PTFE-D2 and ~3.82−3.85 for the Nafion at 20 wt % water content and 2.01 for the PTFE-D2 and 3.40 for the sulfonic Dendrion at 10 wt % water content). At least part of the explanation is that the equivalent weight for PTFE-D2 (~660) is about half that for the Nafion and the Dendrion (~1200). Thus, the PTFE-D2 has a higher sulfonic acid group density than the other two, making it plausible that the structure in the water phase for the PTFE-D2 is perturbed more by the nearly twofold greater number of strong acid groups in the membrane.

3.4. Structure Factors. The differential backbone polymer−water interactions discussed above should be reflected in the phase segregation of the dendrimer-grafted polymer membrane. To provide a quantitative measure of the extent of nanophase segregation that can, in principle, be extracted from the experiment, we calculated the structure factor, $S(q)$, that would be observed in small angle scattering experiments (small angle X-ray scattering, SAXS, and small angle neutron scattering, SANS) using the following equation.

$$\mathbf{S}(\mathbf{q}) = \langle \sum_{r_i} \sum_{r_j} \exp(i\mathbf{q}\cdot\mathbf{r}_{ij})(\xi^i \xi^j - \langle \xi \rangle^2) \rangle / L^3 \qquad (3)$$

where the angular bracket denotes a thermal statistical average, ξ^i represents a local density contrast, $(\phi_A{}^j - \phi_B{}^j)$, $\mathbf{q}$ is the scattering vector, and $\mathbf{r}_{ij}$ is the vector between the site i and the site j. This analysis has been used successfully to investigate the phase segregation in our previous studies on the hydrated membrane for the Nafion[12] and the Dendrion.[11] The SAXS experiments measure the electron density contrast while SANS experiments measure deuterium density contrast. For our analysis, we assigned an artificial density contrast. The local density variables are as follows: $\phi_A{}^j$ is equal to 1 if the site j is occupied by a hydrophilic entity such as water or an acid group and is equal to 0 otherwise, and $\phi_B{}^j$ is equal to 1 if the site is occupied by hydrophobic entities such as the PTFE backbone and is equal to 0 otherwise.

The quantity $\mathbf{S}(\mathbf{q})$ is spherically averaged as follows:

$$S(q) = \sum_{|\mathbf{q}|} \mathbf{S}(\mathbf{q}) / \sum_{|\mathbf{q}|} 1 \qquad (4)$$

with $q = (2\pi/L)n$, where $n = 1, 2, 3, \ldots$ and denotes that, for a given n, a spherical shell is taken as $n - 1/2 \leq qL/2\pi \leq n + 1/2$.

Our previous studies for the hydrated Nafion membrane[12] led to a characteristic dimension of nanophase segregation of ~30 Å for a dispersed monomeric sequence and ~50 Å for a blocky monomeric sequence. Similar studies for the hydrated PTFE Dendrion membrane[11] led to a characteristic dimension of ~30 Å.

For the hydrated dendrimer-grafted polymer membranes, we found the structure factor profiles as a function of scattering vector, $\mathbf{q}$, shown in Figure 9. These structure factor profiles were calculated for the large system consisting of 24 polymer chains as mentioned in section 2. This is because the small system consisting of three polymer chains would not allow the structural development of the phase segregation beyond its system size (~36−40 Å corresponding to q = ~0.15−0.17 Å^{-1}).

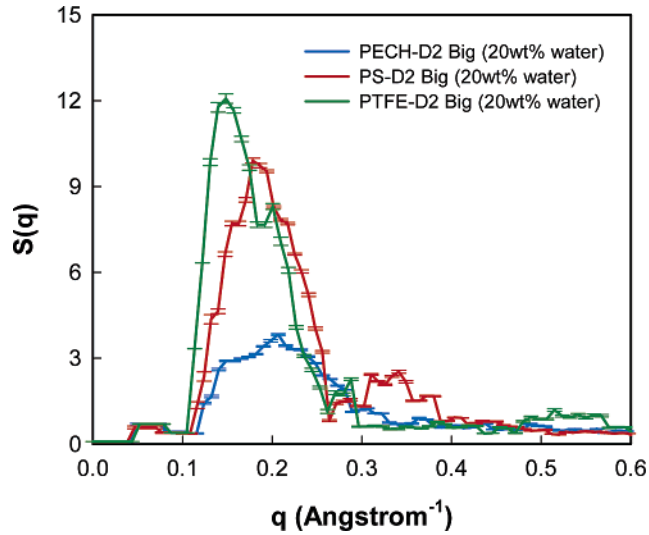

Figure 9. Structure factor profile for hydrated dendrimer-grafted polymer membrane with 20 wt % of water content simulated at 353.15 K. This shows that the characteristic dimension of the nanophase segregated structure is ~20 Å (q = ~0.20 Å^{-1}), ~35 Å (q = ~0.18 Å^{-1}), and ~40 Å (q = ~0.15 Å^{-1}) for PECH-D2, PS-D2, and PTFE-D2, respectively.

At 20 wt % water content, the structure factor analysis in Figure 9 leads to a maximum intensity at ~0.20 Å^{-1} for PECH-D2, corresponding to the characteristic dimension of ~20 Å; ~0.18 Å^{-1} for PS-D2, corresponding to the characteristic dimension of ~35 Å; and ~0.15 Å^{-1} for PTFE-D2, corresponding to the characteristic dimension of ~40 Å. In addition, the intensity of these peaks (indicating the density contrast between hydrophobic domain and water domain) increases in the order of PECH-D2 < PS-D2 < PTFE-D2. From these observations, we conclude that the dimensions of the nanophase segregation is in the order of PECH-D2 < PS-D2 < PTFE-D2. This result from structure factor analysis is very consistent with the analyses (Figures 3, 7, and 8) in previous sections: a more hydrophobic backbone polymer leads to a larger extent of nanophase segregation in the membrane, making the structure in the water phase closer to that in the bulk water.

3.5. Diffusion of Water in the Membrane. Most critical to the performance of PEMFC is the proton conductivity (which we want to be large) and the water diffusion. The proton conductivity is especially dependent on the rotational dynamics of water molecules to facilitate a continuously evolving proton hopping. Although the role of water rotation in the hydrated membrane is essential for a fundamental understanding of proton conduction, it has been little analyzed. Probably, this is due to the lack of experimental tools capable of directly measuring this phenomenon in the membrane. Here, we analyze the rotational water dynamics in the hydrated dendrimer-grafted polymer membrane and compare it with the values computed and measured for bulk water.

A second important feature of water dynamics in the hydrated membrane is the translational diffusion coefficient. If the membrane possesses a high electro-osmotic drag coefficient, it may be necessary to have a high translational diffusion value for water to regulate a uniform water distribution by concentration-gradient-driven drift toward the anode. Inversely, we expect that the electro-osmotic drag of water by the protons would be difficult in an environment having low translational mobility of water. An example is the ice near the melting point where the translational diffusion of water is strongly restricted while the rotational degree of freedom is active.

Previously,[11,12] we showed that the membrane transport properties depend on the extent of nanophase segregation between the hydrophilic and the hydrophobic phase, in agreement with experimental observations.[2,6,57,69] For PEMFC applications, we want to minimize water mobility in order to reduce the electro-osmotic drag of water as protons are transported from anode to cathode. Otherwise, the membrane near the anode can become too dry while the membrane near the cathode floods, producing uneven and unpredictable changes in the conductivity of the membrane during operation of the cell. Thus, we prefer that water in the membrane have a bulk-water-like water phase that percolates throughout the membrane to aid proton transport while simultaneously minimizing translational transport. In this section, we analyze water dynamics from the 5 ns NPT MD simulation in terms of the rotational and translational diffusion.

3.5.1. Rotational Diffusions. To determine the rotational dynamics of water, we calculated the rotational diffusion coefficient (D_R) as[70]

$$D_R = \frac{kTS(0)}{12N} \tag{5}$$

where k is the Boltzmann constant, T is absolute temperature, and N is the number of water molecules. $S(0)$ in eq 5 is the rotational density of states at zero frequency

$$S(\upsilon)]_{\upsilon=0} = \frac{2}{kT}\lim_{\tau\to\infty}\int_{-\tau}^{\tau} C_R(t)e^{-i2\pi\upsilon t}\,dt\Big]_{\upsilon=0} \tag{6}$$

Here, $C_R(t)$ is the autocorrelation function of angular velocity $\omega_{ij}^{CM}(t)$ of water molecule i

$$C_R(t) = \sum_{j=1}^{3} c_{R_j}(t) = \sum_{i=1}^{n}\sum_{j=1}^{3}\langle \omega_{ij}^{CM}(t)\omega ij^{CM}(0)\rangle \tag{7}$$

This analysis allows us to evaluate the rotational diffusion of water molecules in this dendrimer-grafted polymer membrane.

As summarized in Table 3, the calculated rotational diffusion rate (D_R) for bulk water of $(3.25 \pm 0.24) \times 10^{11}$/s is comparable to the experimental value[71] of 2.2×10^{11}/s at the same temperature of 298.15 K. For the higher temperature of 353.15 K, we predict that the D_R value of bulk water increases by a factor of 2.2 (to $7.05 \pm 0.42 \times 10^{11}$/s; we have not found experimental data at this higher temperature).

Table 3 shows that the D_R of water in the dendrimer-grafted polymer membrane increases with increasing water content for all cases in this study. As discussed in section 3.3, the water phase in the hydrated membrane is associated with the strong acid groups of dendrimers to solvate, and the rotation of water molecules that solvate the strong acid groups should be restricted because of the charge-dipole interaction between strong acid groups and solvating water molecules. Considering that the system with higher water content has more water molecules not involved directly in solvating strong acid groups in comparison to that with lower water content, we find it reasonable that the system with a higher water content has a larger value of D_R than that with lower water content. Moreover, this explanation also implies that as the water content increases, the structure in the water phase approaches that in bulk water since the portion of solvating water decreases in that water phase.

We find that the D_R of water increases in the order of PECH-D2 < PS-D2 < PTFE-D2 at the same water content. We attribute this result to the difference in the nanophase segregation for each backbone polymer: the larger the scale of the nanophase segregation, the closer the structure in the water phase approaches that in bulk water, and thereby the closer the water rotation in the water phase of the membrane approaches that in bulk water. This result is consistent with our previous discussions in sections 3.3 and 3.4.

TABLE 3: Rotational Diffusion Coefficients (D_R) of Water from the MD Simulations[a]

system			D_R ($\times 10^{11}$/s)	
			$T = 298.15$ K	$T = 353.15$ K
bulk water			3.25 ± 0.24[d] (exptl 2.2)[b]	7.05 ± 0.42[d]
PECH-D2	10 wt % water content			2.66 ± 0.31
	20 wt % water content			3.58 ± 0.33
PS-D2	10 wt % water content			4.44 ± 0.32
	20 wt % water content			5.70 ± 0.33
PTFE-D2	10 wt % water content			4.70 ± 0.30
	20 wt % water content			6.10 ± 0.31
Nafion	dispersed DR = 1.1	20 wt % water content		7.42 ± 0.54[c,d]
	blocky DR = 0.1	20 wt % water content		6.23 ± 0.53[c,d]
sulfonic dendrion	10 wt % water content			7.49 ± 0.45[d]

[a] This is expected to correlate with proton transport rates. [b] Reference 71. [c] Reference 12. [d] Reference 11.

On the other hand, in comparison with our previous results from Nafion ($D_R = \sim 6.2-7.4 \times 10^{11}$/s)[12] and Dendrion ($D_R = 7.5 \times 10^{11}$/s)[11] (Table 3), only the PTFE-D2 membrane with 20 wt % of water content shows a comparable value, $D_R = 6.10 \times 10^{11}$/s. The other five cases have smaller values. As discussed in section 3.3, we believe that this is due to the smaller equivalent weight of dendrimer-grafted polymers. The increased concentration of sulfonic acid groups in the water phase perturbs the structure of the water phase, making it different from bulk water. The consequence is that the water rotation decreases, in consistency with the studies by Paddison and co-workers.[66,72,73]

3.5.2. Translational Diffusions. This analysis of the translational diffusion of water finds the same trend as observed in previous sections: the higher the water content in the membrane, the closer the translational diffusion of water to that of bulk water. The translational diffusion coefficients (D_T) of water are obtained using $\langle (r(t) - r(0))^2\rangle = 6D_T t$ with the linear part of the mean-square displacement (MSD), as in our previous studies.[11,12] These values are summarized in Table 4 which shows that, for all cases, the D_T value of water increases with increasing water content. The calculated values in bulk water are $D_T = (2.69 \pm 0.04) \times 10^{-5}$ cm^2/s at 298.15 K and $(5.98 \pm 0.07) \times 10^{-5}$ cm^2/s at 353.15 K, which agrees reasonably well with the experimental values ($D_T = 2.30 \times 10^{-5}$ cm^2/s at 298.15 K and 6.48×10^{-5} cm^2/s at 353.15 K).[74−76]

We find that for the same water content D_T increases in the order of PECH-D2 < PS-D2 < PTFE-D2 which is the same trend as the scale of nanophase segregation, which is also consistent with the results in the previous sections.

In addition, we compare the D_T value of water in the dendrimer-grafted polymer membrane with those in the Nafion and the Dendrion membrane. All of the membranes simulated

TABLE 4: Translational Diffusion Coefficients (D_T) of Water from the MD Simulations

system			D_T ($\times 10^5$ cm^2/s)	
			$T = 298.15$ K	$T = 353.15$ K
bulk water			2.69 ± 0.04 (exptl 2.30)[a]	5.98 ± 0.07 (exptl 6.48)[a]
PECH-D2	10 wt % water content			0.05 ± 0.03
	20 wt % water content			0.23 ± 0.04
PS-D2	10 wt % water content			0.10 ± 0.04
	20 wt % water content			0.43 ± 0.04
PTFE-D2	10 wt % water content			0.16 ± 0.04
	20 wt % water content			0.57 ± 0.04
Nafion	DR = 1.1	20 wt % water content		1.43 ± 0.07[b] (1.25)[c]
	DR = 0.1	20 wt % water content		1.62 ± 0.05[b] (1.25)[c]
sulfonic dendrion	10 wt % water content			0.37 ± 0.06[b,d]

[a] References 74−76. [b] Reference 12. [c] Reference 88. [d] Reference 11.

in this study have a smaller D_T than Nafion and Dendrion at the same water content, which suggests that they may have reduced the electro-osmotic drag coefficient. As discussed in our previous study on the hydrated Dendrion membrane,[11] the inner structure of hydrophilic dendrimer architecture may work efficiently in reducing the translational mobility of water while retaining the level of its rotational mobility.

In summary, on the basis of the observation that the translational mobility of water in these dendrimer-grafted polymer membranes is at most ∼40% of that in the Nafion, we expect that the electro-osmotic dragging would be less in this new membrane.

4. Proton Transport

In these membranes, protons are transported through two different mechanisms: (i) the diffusion of protonated water molecules (vehicular diffusion) and (ii) the hopping of the proton along sequences of water molecules (Grothuss diffusion).

We calculate vehicular diffusion directly from the MD using

$$D_{\text{vehicular}} = \langle (r(t) - r(0))^2 \rangle / 6t$$

However, the proton hopping involves forming and breaking covalent bonds as a proton moves from one hydronium molecule to a neighboring water molecule. To study this Grothuss diffusion of protons in water, one must use a method of calculating forces that allows bonds to be formed and broken. This has been done using forces from quantum mechanics (QM),[58,59] but such QM−MD is limited to ∼200 atoms, too few for our studies of a hydrated membrane. An alternative is to use the ReaxFF, which leads to the same potential barriers for proton hopping as the QM. This is feasible for systems of 1000 to 10 000 atoms per cell considered here, but we have not parametrized ReaxFF yet for sulfonic and Teflon systems. An alternative approach is the multistate empirical valence bond (MS-EVB) model developed by Voth and co-workers and applied to the proton transport in hydrated membranes.[50,77,78] Another approach has been used by Paddison et al. for the self-diffusion coefficient of protons in an arbitrary membrane channel using their nonequilibrium statistical mechanical framework.[79−82]

Instead, we employ a simple and efficient method based on transition state theory (TST) to estimate the contribution from the proton hopping mechanism to proton diffusion. The QM hopping method has been successful in investigating the proton hopping in the Dendrion membrane.[11]

To calculate the hopping diffusion in the membrane, we first parametrized the rate constant for the transfer of a proton from the protonated water (hydronium) to the neutral carrier as a function of the intermolecular oxygen in donor distance and oxygen in acceptor distance (Figure 13a in ref 11) using the following equation[83,84]

$$k_{ij}(r) = \kappa(T,r)\frac{k_B T}{h}\exp\left(-\frac{E_{ij}(r) - 1/2h\omega(r)}{RT}\right) \qquad (8)$$

where $\kappa(T,r)$ and $\omega(r)$ are the tunneling factor and the frequency for zero point energy correction (given in refs 83 and 84), respectively, and $E(r)$ is the energy barrier for the proton to be transferred from donor to acceptor in the water medium while they are at a distance of r. We calculated this proton hopping energy barrier for fixed distances between donor and acceptor oxygen in oxygen using QM (B3LYP with the 6-311G** basis set) to obtain the energy change as a function of the distance between the proton and the donor oxygen. Then, we used the Poisson−Boltzmann self-consistent reaction field model[85,86] for the solvent effect correction along the reaction path and recalculated the energy barrier.

Given eq 8, we use the distances between all of the pairs of donors and acceptors from the equilibrium MD trajectory to calculate the hopping diffusion coefficient as follows:

$$D_{\text{hopping}} = \frac{1}{6Nt}\int_0^{t\to\infty}\sum_i^N\sum_j^M k_{ij} r_{ij}^2 P_{ij}\,\mathrm{d}t \qquad (9)$$

where N is the number of protons and P_{ij} is the probability with which a proton can jump from hydronium i to water j defined as $P_{ij} = k_{ij}/\sum_j^M k_{ij}$. Here, r_{ij} is the distance between all of the pairs of donors and acceptors measured from the equilibrium MD trajectory.

Table 5 summarizes the proton diffusion coefficients predicted for all of the dendrimer-grafted polymer membranes. We see here that (i) both $D_{\text{vehicular}}$ and D_{hopping} increase with increasing water content and (ii) the diffusion coefficient increases in the order of PECH-D2 < PS-D2 < PTFE-D2 at the same water content.

These observations are completely consistent with the above analyses on the structure and dynamics of water in the water phase, suggesting that the water in the membrane approaches that in bulk water as the nanophase segregation proceeds.

Particularly, the proton diffusion coefficient predicted for PTFE-D2 (0.69×10^{-5} cm^2/s) is comparable with that predicted for Dendrion (0.52×10^{-5} cm^2/s) and for Nafion (∼0.6−0.7 $\times 10^{-5}$ cm^2/s). This latter value is in good agreement with the experimental values (∼0.5−0.7 $\times 10^{-5}$ cm^2/s from Zawodzinski et al.[87] and Kreuer,[56] Table 4). Considering that PTFE-D2 has the same backbone polymer as Nafion and Dendrion, we find this result on proton transport confirms the importance of the structure in the water phase of the membrane and the relationship between the nanophase segregation and the structure and dynamics in the water phase. Here, it should be noted that we used an ad hoc assumption of $D_{\text{total}} = D_{\text{vehicular}} + D_{\text{hopping}}$ to

TABLE 5: Proton Diffusion Coefficients (*D*)

system ($T = 353.15$ K)			$D_{vehicular}$ (10^{-5} cm^2/s)	$D_{hopping}$ (10^{-5} cm^2/s)	D_{total} (10^{-5} cm^2/s)
PECH-D2	10 wt % water content		0.002	0.300	0.302
	20 wt % water content		0.017	0.379	0.396
PS-D2	10 wt % water content		0.005	0.331	0.336
	20 wt % water content		0.018	0.447	0.465
PTFE-D2	10 wt % water content		0.015	0.440	0.455
	20 wt % water content		0.128	0.563	0.691
Nafion	DR = 1.1	20 wt % water content	0.290[a]	0.342[b]	0.632[b] (exptl ~0.5−0.7)[c]
	DR = 0.1	20 wt % water content	0.294[a]	0.407[b]	0.701[b] (exptl ~0.5−0.7)[c]
sulfonic dendrion	10 wt % water content		0.141[b]	0.377[b]	0.518[b]

[a] Reference 12. [b] Reference 11. [c] References 56 and 87.

predict the overall proton diffusion coefficient (D_{total}). Although this assumption has not yet been thoroughly validated, we believe that the order of the proton diffusion coefficient (PECH-D2 < PS-D2 < PTFE-D2) should be reasonable in our systems in which the hopping mechanism is much more dominant in comparison to the vehicular mechanism. We leave the evaluation/refinement of this assumption to future work.

5. Summary

This study introduced the concept of a dendrimer-grafted polymer using precisely defined water-soluble dendritic architecture (sulfonic polyaryl ether dendrimer) in a copolymer with a linear polymer backbone for applications such as PEMFC. In order to investigate the effect of the backbone polymer on the properties suitable for PEMFC such as nanophase segregation and transport, we grafted the second-generation sulfonic polyaryl ether dendrimers onto three different types of linear backbone polymers, for example, PECH, PS, and PTFE, for the preparation of three different types of dendrimer-grafted polymers such as PECH-D2, PS-D2, and PTFE-D2.

We found that, in all of these cases, the equilibrium systems exhibit nanophase segregation in which a water phase is formed and associated with the hydrophilic dendrimers. Analyzing the pair correlation of sulfur−sulfur in sulfonic acid groups of dendrimers, we found that, in the nanophase-segregated structures, the dendrimers contact each other through the membrane, helping the formation of a continuous and percolated water phase.

We also found out that the water coordination number for water molecules in the water phase increases with increasing water content for all cases. In addition, at the same water content, the water coordination number increases in the order of PECH-D2 < PS-D2 < PTFE-D2, indicating that the similarity of the water structure to the bulk water is also in the order of PECH-D2 < PS-D2 < PTFE-D2.

The extent of nanophase segregation in the new copolymer membrane was evaluated quantitatively by analyzing structure factor profiles, $S(q)$, as a function of scattering vector (**q**) for the membranes with 20 wt % of water content. By determining the characteristic dimension and density contrast in the membrane, we found that the extent of nanophase segregation increases in the order of PECH-D2 (~20 Å) < PS-D2 (~35 Å) < PTFE-D2 (~40 Å) which can be compared to ~30−50 Å for Nafion and ~30 Å for Dendrion.

We suggest that the structure of the water phase and the structure factor analysis can be understood in terms of the hydrophilicity (or hydrophobicity) of the backbone polymer: as the hydrophobicity of the backbone increases, the corresponding membrane develops more nanophase segregation accompanied with a more bulk-water-like structure.

Calculating the rotational diffusion coefficient (D_R) and the translational diffusion coefficient (D_T) from the MD trajectory files, we found that the values of these diffusion coefficients increase with increasing water content and increase in the order of PECH-D2 < PS-D2 < PTFE-D2 at the same water content, indicating that the water dynamics in the hydrated membrane is strongly coupled with the structures in water phase.

We estimated the proton diffusion according to its mechanism: vehicular and hopping. For both mechanisms, the values of the proton diffusion coefficients increase with increasing water content and increase in the order of PECH-D2 < PS-D2 < PTFE-D2, which also shows the dependency of proton transport on the structures in the water phase as observed in the water dynamics.

On the basis of the observations from our simulations, we expect that the PTFE-D2 dendrimer-grafted polymer membrane may have a comparable performance to Nafion and Dendrion membranes in a PEMFC.

Acknowledgment. We thank Dr. Suhas Niyogi and Dr. Deborah Myers of the Argonne National Laboratory and Dr. Gerald Voecks and Dr. Boris Merinov for many helpful discussions. Partial support for this project was provided by DOE (DE-FG01-04ER04-20) and NSF (CTS-0548774). The facilities of the Materials and Process Simulation Center used for these studies are supported by DURIP-ARO and DURIP-ONR, and other support for the MSC comes from MURI-ARO, MURI-ONR, DOE, ONR, NSF-CSEM, NIH, General Motors, Chevron-Texaco, Seiko-Epson, Beckman Institute, and Asahi Kasei.

References and Notes

(1) Carrette, L.; Friedrich, K. A.; Stimming, U. *ChemPhysChem* **2000**, *1*, 162−193.

(2) Kreuer, K. D. *J. Membr. Sci.* **2001**, *185*, 29−39.
(3) Paddison, S. J. *Annu. Rev. Mater. Res.* **2003**, *33*, 289−319.
(4) Li, Q.; He, R.; Jensen, J. O.; Bjerrum, N. J. *Chem. Mater.* **2003**, *15*, 4896−4915.
(5) Maurits, K. A.; Moore, R. B. *Chem. Rev.* **2004**, *104*, 4535−4585.
(6) Hickner, M. A.; Pivovar, B. S. *Fuel Cells (Weinheim, Ger.)* **2005**, *5*, 213−229.
(7) Yeager, H. L.; Steck, A. *Anal. Chem.* **1979**, *51*, 862−865.
(8) Yeo, S. C.; Eisenberg, A. *J. Appl. Polym. Sci.* **1977**, *21*, 875−898.
(9) Eisenberg, A.; King, M. In *Polymer Physics;* Stein, R. S., Ed.; Academic Press: New York, 1977.
(10) Scibona, G.; Fabiani, C.; Scuppa, B. *J. Membr. Sci.* **1983**, *16*, 37−50.
(11) Jang, S. S.; Lin, S.-T.; Cagin, T.; Molinero, V.; Goddard, W. A., III. *J. Phys. Chem. B* **2005**, *109*, 10154−10167.
(12) Jang, S. S.; Molinero, V.; Cagin, T.; Goddard, W. A., III. *J. Phys. Chem. B* **2004**, *108*, 3149−3157.
(13) Mayo, S. L.; Olafson, B. D.; Goddard, W. A., III. *J. Phys. Chem.* **1990**, *94*, 8897−8909.
(14) Elliott, J. A.; Hanna, S.; Elliott, A. M. S.; Cooley, G. E. *Phys. Chem. Chem. Phys.* **1999**, *1*, 4855−4863.
(15) Vishnyakov, A.; Neimark, A. V. *J. Phys. Chem. B* **2000**, *104*, 4471−4478.
(16) Vishnyakov, A.; Neimark, A. V. *J. Phys. Chem. B* **2001**, *105*, 7830−7834.
(17) Li, T.; Wlaschin, A.; Balbuena, P. B. *Ind. Eng. Chem. Res.* **2001**, *40*, 4789−4800.
(18) Jang, S. S.; Blanco, M.; Goddard, W. A., III; Caldwell, G.; Ross, R. B. *Macromolecules* **2003**, *36*, 5331−5341.
(19) Levitt, M.; Hirshberg, M.; Sharon, R.; Laidig, K. E.; Daggett, V. *J. Phys. Chem. B* **1997**, *101*, 5051−5061.
(20) Rappe, A. K.; Goddard, W. A., III. *J. Phys. Chem.* **1991**, *95*, 3358−3363.
(21) Hockney, R. W.; Eastwood, J. W. *Computer simulation using particles;* McGraw-Hill: New York, 1981.
(22) Plimpton, S. J. *J. Comput. Phys.* **1995**, *117*, 1−19.
(23) Plimpton, S. J.; Pollock, R.; Stevens, M. Presented at the Eighth SIAM Conference on Parallel Processing for Scientific Computing, Minneapolis, MN, 1997.
(24) Jang, S. S.; Lin, S.-T.; Maiti, P. K.; Blanco, M.; Goddard, W. A., III; Shuler, P.; Tang, Y. *J. Phys. Chem. B* **2004**, *108*, 12130−12140.
(25) Swope, W. C.; Andersen, H. C.; Berens, P. H.; Wilson, K. R. *J. Chem. Phys.* **1982**, *76*, 637−649.
(26) Laporta, M.; Pegoraro, M.; Zanderighi, L. *Phys. Chem. Chem. Phys.* **1999**, *1*, 4619−4628.
(27) *Cerius2 Modeling Environment*, Release 4.0; Accelrys Inc.: San Diego, CA, 1999.
(28) Nose, S. *J. Chem. Phys.* **1984**, *81*, 511−519.
(29) Eisenberg, A. *Macromolecules* **1970**, *3*, 147−154.
(30) Falk, M. *Can. J. Chem.* **1980**, *58*, 1495−1501.
(31) Duplessix, R.; Escoubes, M.; Rodmacq, B.; Volino, F.; Roche, E.; Eisenberg, A.; Peneri, M. *Water in Polymer;* American Chemical Soceity: Washington, D.C., 1980.
(32) Rodmacq, B.; Coey, J. M.; Escoubes, M.; Roche, E.; Duplessix, R.; Eisenberg, A.; Pineri, M. In *Water in Polymers;* Rowland, S. P., Ed.; American Chemical Soceity: Washington, DC, 1980.
(33) Gierke, T. D.; Munn, G. E.; Wilson, F. C. *J. Polym. Sci., Polym. Phys. Ed.* **1981**, *19*, 1687−1704.
(34) Hsu, W. Y.; Gierke, T. D. *J. Membr. Sci.* **1983**, *13*, 307−326.
(35) Yeager, H. L.; Steck, A. *J. Electrochem. Soc.* **1981**, *128*, 1880−1884.
(36) Verbrugge, M. W.; Hill, R. F. *J. Electrochem. Soc.* **1990**, *137*, 886−893.
(37) Gebel, G. *Polymer* **2000**, *41*, 5829−5838.
(38) James, P. J.; Elliott, J. A.; McMaster, T. J.; Miles, J. M. *J. Mater. Sci.* **2000**, *35*, 5111−5119.
(39) James, P. J.; McMaster, T. J.; Newton, J. M.; Miles, M. J. *Polymer* **2000**, *41*, 4223−4231.
(40) Haubold, H.-G.; Vad, T.; Jungbluth, H.; Hiller, P. *Electrochim. Acta* **2001**, *46*, 1559−1563.
(41) Rollet, A.-L.; Gebel, G.; Simonin, J.-P.; Turq, P. *J. Polym. Sci., Part B: Polym. Phys.* **2001**, *39*, 548−558.
(42) Rollet, A.-L.; Diat, O.; Gebel, G. *J. Phys. Chem. B* **2002**, *106*, 3033−3036.
(43) Young, S. K.; Trevino, S. F.; Tan, N. C. B. *J. Polym. Sci., Part B: Polym. Phys.* **2002**, *40*, 387−400.
(44) Tovbin, Y. K.; Dyakov, Y. A.; Vasutkin, N. F. *Russ. J. Phys. Chem. (Engl. Transl.)* **1993**, *67*, 2122−2125.
(45) Dyakov, Y. A.; Tovbin, Y. K. *Russ. Chem. Bull.* **1995**, *44*, 1233−1236.
(46) Din, X.-D.; Michaelides, E. E. *AIChE J.* **1998**, *44*, 35−47.
(47) Vishnyakov, A.; Neimark, A. V. *J. Phys. Chem. B* **2001**, *105*, 9586−9594.
(48) Jinnouchi, R.; Okazaki, K. *J. Electrochem. Soc.* **2003**, *150*, E66−E73.
(49) Paddison, S. J.; Elliott, J. A. *J. Phys. Chem. A* **2005**, *109*, 7583−7593.
(50) Petersen, M. K.; Wang, F.; Blake, N. P.; Metiu, H.; Voth, G. A. *J. Phys. Chem. B* **2005**, *109*, 3727−3730.
(51) Blake, N. P.; Petersen, M. K.; Voth, G. A.; Metiu, H. *J. Phys. Chem. B* **2005**, *109*, 24244−24253.
(52) Hawker, C. J.; Wooley, K. L.; Frechet, J. M. J. *J. Chem. Soc., Perkin Trans. 1* **1993**, 1287−1297.
(53) Agmon, N. *Chem. Phys. Lett.* **1995**, *244*, 456−462.
(54) Agmon, N.; Goldberg, S. Y.; Huppert, D. *J. Mol. Liq.* **1995**, *64*, 161−195.
(55) Kreuer, K. D. *Chem. Mater.* **1996**, *8*, 610−641.
(56) Kreuer, K. D. *Solid State Ionics* **1997**, *97*, 1−15.
(57) Kreuer, K. D. *Solid State Ionics* **2000**, *136*−137, 149−160.
(58) Tuckerman, M.; Laasonen, K.; Sprik, M.; Parrinello, M. *J. Chem. Phys.* **1995**, *103*, 150−161.
(59) Tuckerman, M.; Laasonen, K.; Sprik, M.; Parrinello, M. *J. Phys. Chem.* **1995**, *99*, 5749−5752.
(60) Tuckerman, M. E.; Marx, D.; Klein, M. L.; Parrinello, M. *Science* **1997**, *275*, 817−820.
(61) Marx, D.; Tuckerman, M. E.; Hutter, J.; Parrinello, M. *Nature* **1999**, *397*, 601−604.
(62) Marx, D.; Tuckerman, M. E.; Parrinello, M. *J. Phys.: Condens. Matter* **2000**, *12*, A153−A159.
(63) Verbrugge, M. W.; Hill, R. F. *J. Electrochem. Soc.* **1990**, *137*, 893−899.
(64) Verbrugge, M. W.; Hill, R. F. *J. Electrochem. Soc.* **1990**, *137*, 3770−3777.
(65) Zawodzinski, T. A.; Neeman, M.; Sillerud, L. O.; Gottesfeld, S. *J. Phys. Chem.* **1991**, *95*, 6040−6044.
(66) Paul, R.; Paddison, S. J. *J. Phys. Chem. B* **2004**, *108*, 13231−13241.
(67) Soper, A. K.; Phillips, M. G. *Chem. Phys.* **1986**, *107*, 47−60.
(68) Farid, A. S. *Plast., Rubber Compos.* **1999**, *28*, 346−356.
(69) Schuster, M.; Kreuer, K. D.; Maier, J. Proceedings of the 14th International Conference on Solid State Ionics, Monterey, CA, 2003; p 395.
(70) McQuarrie, A. A. *Statistical Mechanics;* Harper & Row: New York, 1976.
(71) Pal, S. K.; Peon, J.; Bagchi, B.; Zewail, A. H. *J. Phys. Chem. B* **2002**, *106*, 12376−12395.
(72) Paddison, S. J.; Reagor, D. W.; Zawodzinski, T. A. *J. Electroanal. Chem.* **1998**, *459*, 91−97.
(73) Paddison, S. J.; Bender, G.; Kreuer, K. D.; Nicoloso, N.; Zawodzinski, T. A. *J. New Mater. Electrochem. Syst.* **2000**, *3*, 291−300.
(74) Mills, R. *J. Phys. Chem.* **1973**, *77*, 685−688.
(75) Krynicki, K.; Green, C. D.; Sawyer, D. W. *Discuss. Faraday Soc.* **1978**, *66*, 199−208.
(76) Price, W. S.; Ide, H.; Arata, Y. *J. Phys. Chem. A* **1999**, *103*, 448−450.
(77) Schmitt, U. W.; Voth, G. A. *J. Phys. Chem. B* **1998**, *102*, 5547−5551.
(78) Schmitt, U. W.; Voth, G. A. *J. Chem. Phys.* **1999**, *111*, 9361−9381.
(79) Paddison, S. J.; Paul, R.; Zawodzinski, T. A. *J. Electrochem. Soc.* **2000**, *147*, 617−626.
(80) Paddison, S. J.; Paul, R.; Zawodzinski, T. A. *J. Chem. Phys.* **2001**, *115*, 7753−7761.
(81) Paddison, S. J.; Paul, R.; Kreuer, K.-D. *Phys. Chem. Chem. Phys.* **2002**, *4*, 1151−1157.
(82) Paddison, S. J.; Paul, R. *Phys. Chem. Chem. Phys.* **2002**, *4*, 1158−1163.
(83) Lill, M. A.; Helms, V. *J. Chem. Phys.* **2001**, *114*, 1125−1132.
(84) Lill, M. A.; Helms, V. *J. Chem. Phys.* **2001**, *115*, 7985−7992.
(85) Greeley, B. H.; Russo, T. V.; Mainz, D. T.; Friesner, R. A.; Langlois, J. M.; Goddard, W. A., III; Donnelly, R. E.; Ringnalda, M. N. *J. Chem. Phys.* **1994**, *101*, 4028−4041.
(86) Marten, B.; Kim, K.; Cortis, C.; Friesner, R. A.; Murphy, R. B.; Ringnalda, M. N.; Sitkoff, D.; Honig, B. *J. Phys. Chem.* **1996**, *100*, 11775−11788.
(87) Zawodzinski, T. A.; Springer, T. E.; Davey, J.; Jestel, R.; Lopez, C.; Valerio, J.; Gottesfeld, S. *Electrochim. Acta* **1995**, *40*, 297−302.
(88) Okada, T.; Xie, G.; Meeg, M. *Electrochim. Acta* **1998**, *14*, 2141−2155.